THE JOURNAL OF PHYSICAL CHEMISTRY A

Article

pubs.acs.org/JPCA

Resonance IR: A Coherent Multidimensional Analogue of Resonance Raman

Erin S. Boyle, Nathan A. Neff-Mallon, Jonathan D. Handali, and John C. Wright*

Department of Chemistry, University of Wisconsin—Madison, 1101 University Avenue, Madison, Wisconsin 53706, United States

Supporting Information

ABSTRACT: This work demonstrates the use of triply resonant sum frequency (TRSF) spectroscopy as a "resonance IR" analogue to resonance Raman spectroscopy. TRSF is a four-wave-mixing process where three lasers with independent frequencies interact coherently with a sample to generate an output at their triple summation frequency. The first two lasers are in the infrared and result in two vibrational excitations, while the third laser is visible and induces a two-quantum anti-Stokes resonance Raman transition. The signal intensity grows when the laser frequencies are all in resonance with coupled vibrational and electronic states. The method therefore provides electronic enhancement of IR-active vibrational modes. These modes may be buried beneath solvent in the IR spectrum and also be Raman-inactive and therefore inaccessible by other techniques. The method is presented on the centrosymmetric complex copper phthalocyanine tetrasulfonate. In this study, the two vibrational frequencies were scanned across ring-breathing modes, while the visible frequency was left in resonance with the copper phthalocyanine tetrasulfonate Q band, resulting in a two-dimensional infrared plot that also reveals coupling between vibrational states. TRSF has the potential to be a very useful probe of structurally similar biological motifs such as hemes, as well as synthetic transition-metal complexes.

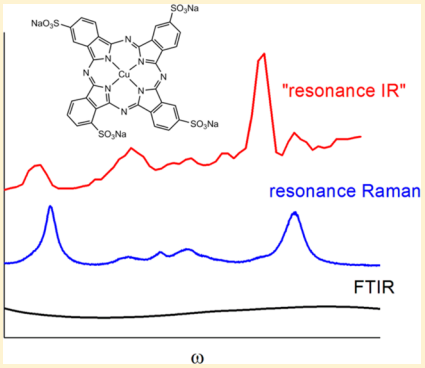

INTRODUCTION

The discovery of the resonance Raman effect was a critical advancement for Raman spectroscopy. By using an excitation frequency that was resonant with an electronic transition coupled to the vibrations of interest, Raman intensity of vibrational modes coupled to that electronic transition could be increased by up to 6 orders of magnitude.[1] This increase allowed the collection of vibrational spectra on dilute species with little background. Resonance Raman spectroscopy is now used extensively to unambiguously define the functionality and bond order of coordinating species in transition-metal complexes.[2,3] A Raman excitation profile, similarly, assists in the assignment of electronic states[4,5] because electronic transitions most strongly enhance the vibrations whose electron density changes.[2] This information aids greatly in the determination of both the ground and excited electronic state structure[6] and is used to verify computational models of molecular systems.[7] However, in molecules with high symmetry, selection rules result in many vibrational modes being Raman-inactive and therefore invisible to resonance Raman spectroscopy. Even in molecules of lower symmetry, it is common for Raman and infrared intensities to be very different for a given vibrational mode. Thus, IR and Raman techniques provide complementary information about molecular vibrations. Infrared spectra often have strong solvent and cosolute absorption in the mid-infrared; therefore, viewing particular IR-active modes can be difficult or impossible without the benefit of electronic enhancement.

Such is the case for tetrasulfonated copper phthalocyanine ($Cu(tsPc)^{4-}$) in D_2O. Phthalocyanines belong to the porphyrin family, a class of molecules that is of broad interest due to their appearance in proteins such as hemoglobin and cytochromes, as well as their growing importance in areas including catalytic redox reactions,[8] photosensitization in solar cells,[9] and molecular electronics.[10] Like porphyrins, phthalocyanine molecules are centrosymmetric when they are unsubstituted or when substitution maintains their inversion symmetry. Because of this symmetry, vibrational infrared and Raman activity are mutually exclusive.

Though the $Cu(tsPc)^{4-}$ (Figure 1) used here has one sulfonate substituent placed at a different position than the others, breaking perfect inversion symmetry, it maintains mutually exclusive IR and Raman modes and will therefore be referred to as centrosymmetric for the purpose of this paper. In this study, we demonstrate the use of triply resonant sum frequency (TRSF) spectroscopy on $Cu(tsPc)^{4-}$ as a "resonance IR" analogue to resonance Raman spectroscopy.

TRSF spectroscopy is a four-wave mixing technique belonging to the field of coherent multidimensional spectroscopy (CMDS). CMDS is an emerging field that is the optical analogue to multidimensional NMR.[11−14] Just as multidimensional NMR observes coupling between nuclear spin states,

Received: February 21, 2014
Revised: April 3, 2014
Published: April 7, 2014

   dx.doi.org/10.1021/jp5018554 | J. Phys. Chem. A 2014, 118, 3112−3119

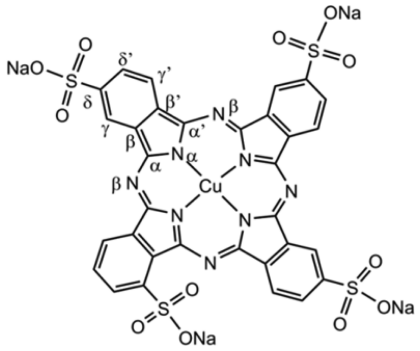

Figure 1. Copper phthalocyanine-3,4′,4″,4‴-tetrasulfonic acid tetrasodium salt. Greek letters assign the nitrogen and carbon atoms following the convention of ref 10.

CMDS probes the coupling between various vibrational or electronic quantum states within a sample. This information has similarly aided the understanding of molecular structure[15] and heterogeneity,[16] as well as allowing observation of dynamics occurring on time scales faster than NMR can resolve (fs−ns).[12,16]

CMDS uses pulsed, coherent excitation fields to create time-dependent superpositions of quantum states in the chemical system. Coupled pairs of states form "coherences" that launch coherent, directional light fields at the frequency difference between the states in the pair. Because these output fields obey conservation of momentum, the direction of the output beam is defined by the phase and multiplicity of the interactions of the excitation pulses. The ability for a pulse sequence to generate output intensity depends on the success of phase-matching between the vector sum of the excitation pulses and the wave vector of the output beam. It also relies upon the coupling between the states involved in the pathway chosen. This coupling relates to molecular structure and is the source of the information learned in CMDS.[11]

The most common implementation of CMDS experiments is in the time domain. In these experiments, broad-band pulses cover the frequency range of interest. Spectral information is obtained by heterodyning the output with a local oscillator, scanning the time delays between the pulses, and Fourier transforming the signals to the frequency domain.[11] Although this is an efficient implementation strategy, it is spectrally limited to the range of quantum states accessible within the pulse bandwidths. The inability to maintain shot-to-shot phase stability[17] across laser sources of different colors also requires three-color experiments in the time domain to use higher-order and less-efficient $\chi^{(5)}$ processes.

The methodology presented here belongs to an alternative class of CMDS experiments, performed in mixed frequency−time domain. These experiments employ pulses with spectral and temporal widths matching the dephasing times of relevant states. In such a design, each pulse is spectrally narrow enough to excite only one state while still maintaining a rigorous time ordering of the interactions. Spectra are collected by scanning frequencies, and coherent and incoherent dynamics can be measured by scanning pulse delays. Either fully coherent or population pathways can be chosen, using frequencies resonant with any vibrational and electronic states.[12,13,18,19]

TRSF spectroscopy uses a series of three excitation pulses to create a triple quantum coherence involving two vibrational states and an electronic state. It employs the phase-matching condition $\vec{k}_s = \vec{k}_1 + \vec{k}_2 + \vec{k}_3$, where the subscripts represent the

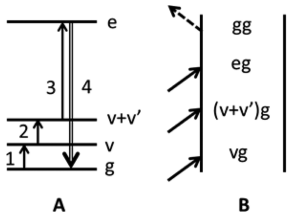

Figure 2. TRSF pathway represented as (A) a WMEL diagram and (B) a Feynman diagram.

excitation fields defined by their frequencies ω_1, ω_2, and ω_3 (rather than their time ordering). Defining a TRSF time ordering also defines a unique, fully coherent pathway. For example, Figure 2a demonstrates the pathway $gg \xrightarrow{1} \nu g \xrightarrow{2} (\nu + \nu')g \xrightarrow{3} eg$ via a wave-mixing energy level (WMEL) diagram, where time moves left to right, ket side transitions are represented by solid arrows (bra side would be represented by dashed arrows, were there any), and horizontal lines represent quantum states. Figure 2b presents the same pathway via a Feynman diagram, where time moves bottom to top, ket side transitions occur on the left side of the diagram, excitation arrows point toward the states, and emissive transitions point away. Here, ω_1 excites fundamental vibrational modes, ν, ω_2 excites overtone and combination band modes ($\nu + \nu'$), and ω_3 excites the electronic state, which generates a coherent resonance Raman transition returning the system to the ground state (interactions 3 and 4). The ω_1 and ω_2 transitions follow infrared selection rules.

The nonelectronically resonant triple sum frequency (TSF)[20] pathway, which employs the same phase-matching condition, would have a dashed line representing a virtual electronic state "e" in the WMEL diagram. The difference between these pathways is completely analogous to the difference between resonant and nonresonant Raman scattering, and interesting results of that difference have been described elsewhere.[20,21] Briefly, both pathways climb the vibrational ladder with the first two infrared laser interactions, and the final visible interaction causes a two-quantum Raman transition. In nonresonant Raman scattering, selection rules are important, and transitions with $\Delta\nu \neq 1$ become very weak. When they do occur, it is often due to coupling between the $(\nu + \nu')$ overtone or combination band and a fundamental mode in the same region, a Fermi resonance. In resonance Raman, however, the intensity of overtone and combination band transitions can still be quite strong if the potential energy surface associated with a given vibration is significantly different in the excited electronic state than that in the ground state, and terms like Franck−Condon factors and higher-order components of the Herzberg−Teller expansion become important.[2,5] The result of the electronic resonance is that TRSF spectroscopy allows for observation of mechanical and electronic coupling between any IR-active vibrational modes that are coupled through the electronic state.

Some advantages of the TRSF pathway over a fully infrared method are suppression of signal from solvent and cosolutes that are not electronically resonant, an output frequency unique from the inputs and therefore spectrally separable from scatter, and up-conversion of the vibrational data to a spectral region with more efficient detectors. In this study, these advantages assist in obtaining electronically enhanced, two-dimensional resonance IR spectra of the centrosymmetric complex Cu(tsPc)$^{4-}$.

dx.doi.org/10.1021/jp5018554 | J. Phys. Chem. A 2014, 118, 3112−3119

THEORY AND MODELING

The TRSF output intensity in the steady state is defined by a typical four-wave mixing proportionality,

$$I_{\mathrm{TRSF}} \propto |\chi^{(3)}|^2 l^2 M I_1 I_2 I_3 \tag{1}$$

where l is path length, M is a correction factor discussed below,

$$\chi^{(3)} \propto \frac{N\mu_{\nu g}\mu_{(\nu+\nu')\nu}\mu_{e(\nu+\nu')}\mu_{ge}}{\Delta_1\Delta_2\Delta_3} \tag{2}$$

N is the density of oscillators, $\Delta_i \equiv \delta_{mn} - i\Gamma_{mn}$ is the complex detuning factor, δ_{mn}, μ_{mn}, and Γ_{mn} represent the detuning of the ith excitation frequency from resonance, the transition dipole, and the dephasing rate of the mn coherence. As the laser frequency approaches the frequency difference between the eigenstates m and n, resonance is achieved, and the Δ_i detuning denominator is minimized, maximizing intensity. This equation provides a closed form representation of the resonance enhancements, but it does not account for the time-dependent nature of relative peak intensities when the dephasing rates are comparable with the excitation pulse width. Quantitative modeling requires numerical integration of the time-dependent Schrodinger equation.[20] Note that typical vibrational transition dipole moments $\mu_{\nu g}$ and $\mu_{(\nu+\nu')\nu}$ are small, but that the vibronic transition dipole moments $\mu_{e(\nu+\nu')}$ and μ_{ge} have the potential to be quite large when the $(\nu + \nu')$ vibrational state couples well to the electronic transition, allowing enhancement of weaker ν and ν' vibrational states that could be difficult to observe in fully vibrational techniques.

To gain an intuitive understanding of when such enhancement would occur, we will take advantage of the direct relationship of the resonances in this equation with absorption coefficients and Raman cross sections.[22] When on-resonance, the output intensity can alternatively be described as

$$I_{\mathrm{TRSF}} \propto \frac{\alpha_1\alpha_2\sigma_{(\nu+\nu')g} l^2}{\Gamma_{\nu g}\Gamma_{\nu' g}} M I_1 I_2 I_3 \tag{3}$$

where α_i is the absorption coefficient of the fundamental or overtone/combination band transitions and $\sigma_{(\nu+\nu')g}$ is the Raman cross section of the $(\nu + \nu')g \rightarrow gg$ transition. Note this Raman cross section incorporates an electronic state dephasing rate, Γ_{eg}.[20] M is a correction factor for absorption and phase-matching changes

$$M = \frac{e^{-\alpha_4 l}\left(1 - e^{\frac{\Delta\alpha l}{2}}\right) + 4e^{\frac{\Delta\alpha l}{2}} \sin^2\left(\frac{\Delta k l}{2}\right)}{\left(\frac{\Delta\alpha l}{2}\right)^2 + (\Delta k l)^2} \tag{4}$$

where α_i are the absorption coefficients at the ith excitation or output frequency, $\Delta\alpha = \alpha_4 - (\alpha_1 + \alpha_2 + \alpha_3)$, and $\Delta\vec{k}$ is the phase-mismatch of the wave vectors. For the TRSF pathway, $\Delta\vec{k} \equiv \vec{k}_1 + \vec{k}_2 + \vec{k}_3 - \vec{k}_4$, where $k_i = (n_i\omega_i/c)$, n_i is the index of refraction of the ith frequency, and c is the speed of light. Equation 4 predicts a decrease in signal as the output $\vec{k}_4$ is absorbed and saturation of nonlinear gain at the path length where inputs $\vec{k}_1$, $\vec{k}_2$, and $\vec{k}_3$ have been absorbed.[22]

In the limit of negligible absorption, the M factor reduces to the familiar $\mathrm{sinc}^2(\Delta k l/2)$ dependence. The TRSF pathway cannot be perfectly phase-matched in systems with normal dispersion (higher index at higher frequency) because the indices of refraction make the $\vec{k}_4$ output wave vector larger than the $\vec{k}_1 + \vec{k}_2 + \vec{k}_3$ nonlinear polarization wave vector. Nevertheless, TRSF has high output intensities because the three resonance enhancements are multiplicative and create a large nonlinear gain over a path length shorter than the inverse of their phase-mismatch, Δk. This gain (eq 3) results from the transition moments of coupled infrared modes (α_1, α_2) and the Raman cross section of the resulting overtone or combination band (σ). Though output intensities were high, small differences in the M factor (eq 4) across the spectral range of our 2D data were observed due to changes in absorption and index of refraction from D_2O vibrations and the $Cu(tsPc)^{4-}$ electronic state. These differences have been modeled in order to obtain data absent of this experimental artifact. We also compared M factor differences between fully infrared four-wave mixing and TRSF experiments performed in D_2O. That comparison indicates that while the overall damping of the signal is smaller in fully infrared experiments, the variation throughout the frequency range is comparable to that in TRSF experiments. A full description is provided in the Supporting Information.

EXPERIMENTAL SECTION

Copper phthalocyanine-3,4′,4″,4‴-tetrasulfonic acid tetrasodium salt (anion denoted $Cu(tsPc)^{4-}$) was obtained from Sigma-Aldrich and used without further purification. Sigma estimates its purity to be 85%. $Cu(tsPc)^{4-}$ was dissolved in D_2O and used without further purification. For TRSF and transmission IR spectra, samples were held between two CaF_2 windows, and the path length was controlled using a Teflon spacer.

The laser system used to collect TRSF spectra has been described previously.[20,21] Briefly, a 1 kHz Spectra-Physics regenerative amplifier was used to pump two independently tunable optical parametric amplifiers (OPAs) to generate ω_1 and ω_2 frequencies in the mid-IR, having a duration of 1 ps, spectral bandwidths of ∼15 cm^{-1}, and pulse energies between 0.5 and 1.5 μJ/pulse. A small portion of the 800 nm light from the amplifier was split to serve as ω_3, having a duration of 1.6 ps and pulse energy of <1 μJ/pulse. The three beams were sent to the sample in a planar beam geometry, with ω_3 entering normal to the sample window and ω_1 and ω_2 ±10° to either side. This beam geometry results in the ω_4 output being collinear with ω_3. The processes corresponding to the phase-matching geometries $2\vec{k}_1 + \vec{k}_3$ and $2\vec{k}_2 + \vec{k}_3$ emerge at slight angles to either side of the desired $\vec{k}_1 + \vec{k}_2 + \vec{k}_3$ and are removed with an aperture. The ω_3 signal is removed from the ω_4 signal by a holographic filter stack and a monochromator with 50 cm^{-1} resolution and measured by a PMT via homodyne detection.

To generate 2D TRSF plots, the ω_1 and ω_2 frequencies were independently scanned over the region 1290−1600 cm^{-1} in 4 cm^{-1} steps with automated, home-built Labview software. This resulted in an $\omega_4 = \omega_1 + \omega_2 + \omega_3$ sum frequency between 637 and 663 nm, resonant with the $Cu(tsPc)^{4-}$ Q band. Delay stages were used to maintain constant time delays between pulses. Without correction, the pulse arrival time at the sample is known to change throughout the spectral range due to varying path length through the $AgGaS_2$ difference frequency crystal. This delay trend is calibrated and automatically counteracted by the delay stages to maintain fixed time delays throughout the 2D scan space. Because different OPA frequencies resulted in different ω_1 and ω_2 pulse powers, data were normalized to ω_1 and ω_2 intensities at each point, according to eq 3. (Data were not normalized to ω_3 because its

dx.doi.org/10.1021/jp5018554 | J. Phys. Chem. A 2014, 118, 3112−3119

intensity remained constant.) Each pixel was averaged for 2000 laser shots.

Geometry optimization and time-dependent density functional theory (TD-DFT) calculations were performed on unsulfonated CuPc using the ORCA 2.9 package.[23] Calculations were performed spin-unrestricted and used a B3LYP/G functional.[24−26] An SV(P)[27] basis and SV/C[28] auxiliary basis were used on all atoms except copper, which was described by a TZV(P)[29] basis. The starting coordinates for optimization were obtained from a published iron oxo phthalocyanine structure with axial ligands removed.[30] Electron density difference maps (EDDMs) of the Q band transition were plotted in PyMol 1.5 at an isosurface value of 0.001 au.

RESULTS/DISCUSSION

The UV/visible spectrum of $Cu(tsPc)^{4-}$ in D_2O shows the Soret band at 333 nm and two overlapping Q bands at 671 and 617 nm. In the literature, the latter two have been assigned to the monomer and the aggregate, respectively.[31,32] The electronic structure of unsulfonated copper phthalocyanine (CuPc) has been studied extensively[33] and will carry over to $Cu(tsPc)^{4-}$. The transitions associated with the Soret band and the Q band primarily involve $a_{2u} \rightarrow 2e_g$ and $a_{1u} \rightarrow 2e_g$ one-electron excitations, respectively. The resulting electron configurations have E_u symmetry and are thus subject to configuration interaction, which causes them to mix according to the Gouterman model.[34] The porphyrin family often exhibits a vibronic sideband, Q_v, to the blue of Q. For $Cu(tsPc)^{4-}$, the Q_v band appears at 608 nm and is often obscured under the aggregation peak.[32] Molar absorptivities for these transitions are in the range of $\sim 5 \times 10^4$ M^{-1} cm^{-1}, varying slightly with concentration and aggregation.[31] Though ligand-to-metal charge transfer (LMCT) can contribute significantly to the Q band transition of metal porphyrins containing metals lighter than Cu^{2+}, in CuPc, the mixing of Cu $3d_\pi$ character into the e_g porphyrin LUMO is predicted to be weak.[33] Therefore, in this complex, the Q band likely corresponds to a relatively pure ligand-based $\pi \rightarrow \pi^*$ transition, an assumption corroborated by our TD-DFT calculations.

The Q band resonance Raman spectrum of $Cu(tsPc)^{4-}$ in water, collected at 647 nm, has two prominent bands at 1337 and 1531 cm^{-1} (Figure 3b) in the fundamental ring-breathing region, similar to CuPc[35,36] (Table 1). The overtone region shows only three very weak modes at 2676, 2723, and 2874 cm^{-1} (see Figure S1, Supporting Information). These modes do not correspond to the combination or overtone bands observed in the TRSF spectrum below.

The infrared spectrum in Figure 3b was collected as an attenuated total reflectance (ATR) spectrum on crystalline $Cu(tsPc)^{4-}$. FTIR measurements of saturated $Cu(tsPc)^{4-}$ in D_2O only weakly resolved the $Cu(tsPc)^{4-}$ features from the D_2O background. An ATR spectrum of 26 mM $Cu(tsPc)^{4-}$ in D_2O had a poor signal/noise ratio, but its solvent-subtracted shape matched the ATR shape very well (see Figure S2, Supporting Information). From this spectrum, we estimate the molar absorptivity of the larger peaks in this range to be between 200 and 600 M^{-1} cm^{-1}.

Table 1 summarizes the primary vibrational frequencies of $Cu(tsPc)^{4-}$ and unsulfonated CuPc between 1300 and 1650 cm^{-1}, which correlate well. The Raman excitation wavelength was 488 nm for the literature CuPc data (between the Q and Soret bands),[10] while the wavelength used for this study was 647 nm, in resonance with the Q band. Spectral differences

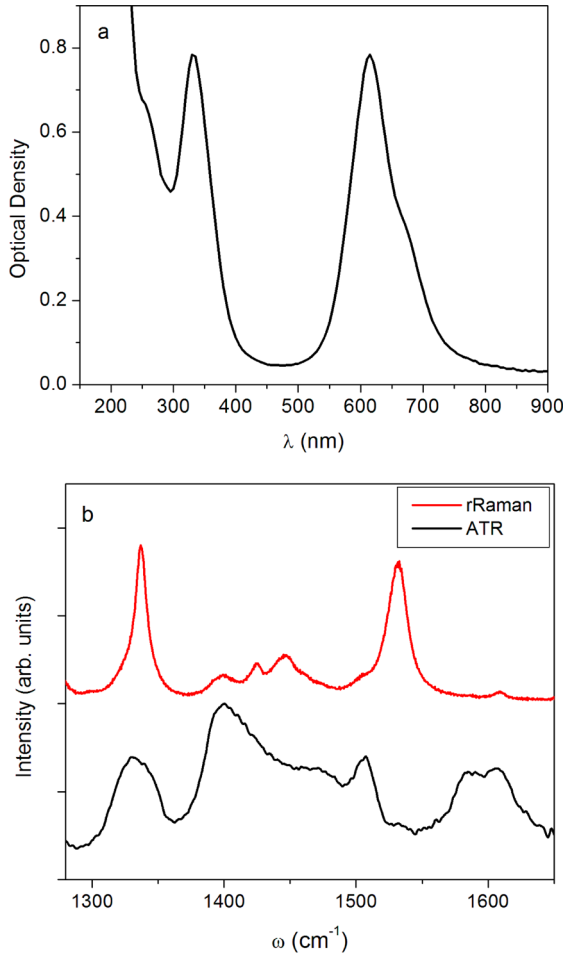

Figure 3. (a) UV/visible absorption spectrum of 25 μm, 5 mM $Cu(tsPc)^{4-}$ in D_2O. (b) Attenuated total reflectance (ATR) infrared spectrum of $Na_4Cu(tsPc)$ solid (black) and the resonance Raman spectrum of 1 mM $Cu(tsPc)^{4-}$ in H_2O at 647 nm (red; offset for clarity).

between CuPc and $Cu(tsPc)^{4-}$ could therefore be due to differences in electronic enhancement in addition to sulfonation. Assignments of the CuPc modes have been made in the literature using DFT and ^{15}N isotopic substitution.[10]

Figure 4 shows the TRSF spectrum of 5 mM $Cu(tsPc)^{4-}$ in D_2O with ω_1 and ω_2 overlapped in time and ω_3 delayed 2.25 ps. The ATR spectrum is plotted above for comparison. The three prominent diagonal features are listed in Table 1, and cross-peaks are observed between these modes. The existence of diagonal and cross-peak features shows that the overtone or combination band couples well to the Q band transition. This is considered within the formalism of Herzberg−Teller coupling below. The raw data were observed to have rising signal intensities at higher frequencies. In order to rule out the possibility of this characteristic arising from phase-mismatch or absorption effects, raw TRSF intensities were divided by the calculated frequency-dependent M factor (eq 2), resulting in the TRSF spectrum shown here. This correction turned out to have minimal qualitative impact on the spectrum. Though it slightly changed relative peak intensities, careful examination shows that the M factor cannot be responsible for the rising intensity observed, which is discussed further below. A full description of the calculation of the M factor is provided in the Supporting Information.

dx.doi.org/10.1021/jp5018554 | J. Phys. Chem. A 2014, 118, 3112−3119

Table 1. Vibrational Frequencies of $Cu(tsPc)^{4-}$ from Current Experiments, With CuPc Vibrations and Assignments from the Literature.[10a]

CuPc[10]	symmetry[10]	assignment[10]	$Cu(tsPc)^{4-}$	TRSF
		IR-Active		
1332	E_u	$C_\beta-C_\beta$, $C_\delta-C_\delta$, isoindole def.	1331	1326
1420	E_u	$N_\beta-C_\alpha$, $C_\beta-C_\beta$, $C_\alpha-C_\beta-C_\beta$, C−C−H, $C_\delta-C_\delta$	1401	1401
1464 (w)	E_u	$N_\beta-C_\alpha$, $C_\beta-C_\beta$, $C_\beta-C_\gamma$, $C_\delta-C_\delta-H$	1465 (b/w)	(a/w)
1507	E_u	$N_\beta-C_\alpha$, $C_\alpha-N_\alpha-C_\alpha$, $C_\alpha-C_\beta$	1507	1506
1589 (w)	E_u	$C_\delta-C_\delta$, $C_\beta-C_\beta$, benzene def., $C_\delta-C_\delta-H$	1585	(a)
1609 (w)	E_u	$C_\beta-C_\gamma$, $C_\gamma-C_\delta$, C−C−H	1606	(a)
		Raman-Active		
1336	A_{1g}	$C_\beta-C_\beta$, $C_\alpha-N_\alpha-C_\alpha$, $C_\beta-C_\gamma$, $C_\gamma-C_\delta$	1337	
(a)	–	–	1400 (b/w)	
1427 (w)	A_{1g}	$C_\beta-C_\beta$, $C_\delta-C_\gamma-H$, $C_\beta-C_\gamma-H$	1425 (w)	
1448	B_{1g}/B_{2g}	$C_\beta-C_\beta$, $C_\beta-C_\gamma-H/C_\alpha-N_\beta$, $N_\alpha-C_\alpha-C_\beta$, C−C−H	1446 (w)	
1481 (w)	A_{2g}	$C_\alpha-N_\beta$, $C_\beta-C_\gamma$, $C_\gamma-C_\delta$	(a)	
1521/1526	A_{1g}/B_{1g}	$C_\alpha-C_\beta$, $C_\alpha-N_\beta$, $C_\beta-C_\beta/C_\alpha-N_\beta$	1531	
1589[b]	B_{1g}	$C_\beta-C_\beta$, $C_\delta-C_\delta$		
1607[b]	A_{1g}	$C_\beta-C_\beta$, $C_\delta-C_\delta$, $C_\delta-C_\delta-H$	1610 (vw)	

[a]Abbreviations: w = weak, b = broad, a = absent. Greek letter assignments of carbon and nitrogen atoms are shown in Figure 1. [b]A mode from literature DFT calculations[10] not observed in resonance Raman.

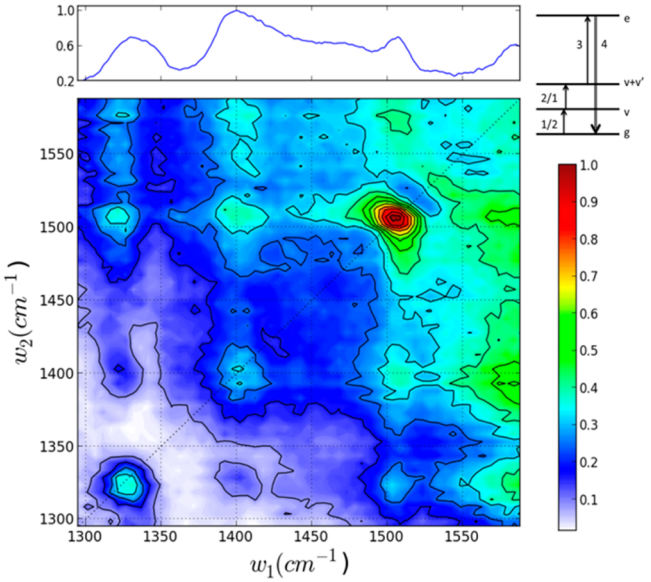

Figure 4. TRSF spectrum of 5 mM $Cu(tsPc)^{4-}$ in D_2O at 25 μm, *M*-factor-corrected. Offset above is the ATR spectrum of crystalline $Na_4Cu(tsPc)$. The WMEL diagram on the top right demonstrates the time ordering of pulses and possible pathways.

TRSF peaks are tabulated in Table 1 and reproduce the ATR maxima well. Differences between these spectra yield information about electronic enhancement because IR absorption depends only on the vibrational transition dipoles while TRSF intensity depends upon a product of vibrational and vibronic transition dipoles (eq 3), as well as pulse delay times, as discussed in the Theory and Modeling section. Therefore, differences in line width can be attributed to underlying modes with differential enhancement in TRSF versus IR absorption. The diagonal peaks at 1589 and 1606 cm^{-1} are not detectable in the TRSF spectrum, even when the scan range is extended (not shown). The rise in signal in this portion of the plot blends smoothly into the rising background at higher frequencies. It is unclear whether cross-peaks exist between these absent diagonal modes and the diagonal peaks observed at lower frequencies. The absence of detectable diagonal features at these frequencies indicates that these modes are not well coupled to the Q band. This explanation is supported by their literature assignment as C=C stretches and C−H bends localized on the outer phenyl rings and not inclusive of stretching on the inner isoindole ring or bridging nitrogen atoms.[10] The DFT-predicted Raman-active modes at nearly the same frequencies have similar assignments and also do not appear in Q band resonance Raman spectra (Figure 3b). The IR modes that we do see in the TRSF spectra all include nitrogen and/or inner isoindole ring deformation according to DFT calculations, leading to the conclusion that the Q band electronic transition involves electron density redistribution on the inner parts of the phthalocyanine macrocycle and does not alter the potential energy surface along the $\nu + \nu'$ vibrational coordinates of the outer benzene rings, preventing their electronic enhancement.

TD-DFT calculations were run to generate EDDMs for the Q band transition, and indeed, these maps indicate that most of the electron density change occurs on the inner porphyrin ring. Additionally, the electron density changes on the inner ring alternate between gain and loss many times while there are only small areas of loss on each outer phenyl ring, resulting in a smaller overall force on these outer nuclei (Figure S3, Supporting Information). Note that these calculations assign essentially all of the Q band transition intensity to changes in ligand-based molecular orbitals, where DFT should perform fairly well.

Because the data in Figure 4 were collected with the two infrared pulses temporally overlapped, two pathways are possible, one where ω_1 excites the fundamental mode and ω_2 excites the combination band and vice versa (see Figure 4, WMEL diagram). When vibrational modes have significant anharmonicity, peaks appear antidiagonal with IR pulses temporally overlapped.[20,21] It is clear that mechanical anharmonicity in this system is small relative to the line width because the peaks in Figure 4 have a Lorentzian line shape. A spectrum with time-delayed pulses therefore was not collected to determine anharmonicities, although this capability has been demonstrated previously.[21]

dx.doi.org/10.1021/jp5018554 | J. Phys. Chem. A 2014, 118, 3112−3119

Minor dispersion is apparent in the line shape of the 1506 cm^{-1} mode, representing interference with a partially resonant TSF[20] background signal. There are two possible sources for this background. Solvent signal in this region is nonzero and will result from both the tail of the O–D bend and the broad, weak D_2O feature centered at 1550 cm^{-1}. These features are not electronically resonant and therefore are weak in comparison to those associated with $Cu(tsPc)^{4-}$ transitions. The stronger source of rising signal intensity in this region is the increasing electronic enhancement at larger ω_1 and ω_2 values as the electronic detuning ($\delta_3 = \omega_1 + \omega_2 + \omega_3 - \omega_e$; eq 2) reaches resonance. Approximating the peak visible absorption $\omega_{vis}{}^0$ as ω_e, electronic resonance maximizes when the ω_1 and ω_2 average frequency is 1815 cm^{-1}, assuming equal coupling for the monomer and aggregate Q band to the vibrational modes. Therefore, the $Cu(tsPc)^{4-}$ modes that are coupled to the Q band will be brighter at the higher-frequency portion of the TRSF scan. In fact, the intensity of the diagonal slice $\omega_1 = \omega_2$ closely follows the profile of the square of the $Cu(tsPc)^{4-}$ absorption spectrum, $\alpha^2(2\omega_1 + \omega_3)$ (see Figure S4 in the Supporting Information). Only the IR-active vibrations that are easily distinguished have been gathered in Table 1, but it is probable that much of the "background" in this region arises from a large number of weakly contributing $Cu(tsPc)^{4-}$ modes that still couple to the Q band.

It is important to note that the $\omega_1 + \omega_2 + \omega_3 - \omega_{vis}{}^0$ resonance criterion serves only as a guide. The TRSF electronic enhancement arises from the $\sigma_{(\nu+\nu')g}$ term in eq 4 that involves an anti-Stokes Raman overtone or combination band. An excitation spectrum of the electronic state would be analogous to a resonance Raman excitation profile with established resonance Raman enhancement terms, which is only approximated as the square of the visible absorption spectrum due to differences in the way each vibrational mode couples to the excited state. In the case of $Cu(tsPc)^{4-}$ (effective D_{4h} symmetry), all IR-active vibrational modes in this region have e_u symmetry,[10] giving their combination bands $a_{1g} + a_{2g} + b_{1g} + b_{2g}$ symmetry by the direct product. Though their gerade symmetry allows their overtones and combination bands to undergo a Raman transition, the fundamental e_u character of the modes precludes the electronic potential energy minima from being displaced significantly along their vibrational coordinate in the excited electronic state. Therefore, the *A* term or Franck–Condon intensity arises primarily from changes in the slope of the potential energy surface in the excited electronic state, an effect that is more significant for overtones and combination bands.[5] This type of enhancement is usually smaller than that associated with excited-state potential displacement[2] but may compete with the other enhancement mechanisms for the two-quantum transitions observed in TRSF because the displacement term is absent. In the case of $Cu(tsPc)^{4-}$, intensity borrowing likely occurs for modes participating in vibronic mixing with another excited electronic state or *B* and *C* term enhancement. This effect is known to occur in the Q_v band of porphyrin systems due to vibronic coupling between the two E_u electronic states arising from the $a_{1u}e_g$ and $a_{2u}e_g$ electron configurations, mediated by the three nontotally symmetric components of gerade symmetry derived from the direct product above.[37]

CONCLUSIONS

In this work, we have demonstrated the use of TRSF spectroscopy, a coherent triple summation pathway, as a resonance IR analogue to resonance Raman spectroscopy. The pathway couples two infrared excitations with a Raman transition that becomes stronger when it is electronically enhanced. Electronic enhancement is obtained when the sum of the input frequencies is resonant with an electronic transition.

This pathway obtains two dimensions of vibrational information, allowing one to parse electronic and mechanical coupling, as has been demonstrated before.[21] The presence of cross-peaks demonstrates the former—coupling of vibrational modes through a shared electronic state. Here, the concerted nuclear motions of the two vibrational modes lead to electronic enhancement of the Raman transition through the Herzberg–Teller terms discussed above. The strength of mechanical coupling manifests as mechanical anharmonicity or the frequency separation between fundamental and overtone/combination band transitions when ω_1 and ω_2 are temporally separated. The $Cu(tsPc)^{4-}$ vibrations in the region investigated display minimal mechanical coupling.

The centrosymmetric molecule $Cu(tsPc)^{4-}$ shares no IR- and Raman-active modes. The IR-active modes were invisible in the sample used for TRSF yet rose above the background in the TRSF spectrum (Figure 4) when coupled to the Q band electronic transition, which has primarily $a_{1u} \rightarrow e_g$ character. The three strongest vibrational transitions in this range met that criterion; however, the benzene deformation modes[10] at 1585 and 1606 cm^{-1} did not appear to be well-coupled to the $a_{1u} \rightarrow e_g$ transition. The pair of gerade modes with similar assignments and frequencies similarly does not appear in the resonance Raman spectrum obtained with excitation into the Q band. Vibrational modes appearing in both the resonance IR spectrum here and the resonance Raman spectrum all contain deformation of β-nitrogens and/or inner isoindole rings,[10] indicating that vibronic coupling to this electronic transition may rely upon such distortions. Indeed, TD-DFT calculations do support the claim that the Q band transition manifests mostly as electronic density changes within the inner porphyrin ring (Figure S3, Supporting Information), demonstrating the ability of TRSF to gain real insight into vibronic coupling. Electronic enhancements in the TRSF pathway rely upon (1) changes to the excited-state potential energy surface slope along the combined vibrational coordinates of the modes constituting the overtone or combination band (*A* term or Franck–Condon factors) and (2) vibronic coupling to another electronic state mediated by the same modes (*B* and *C* term enhancement).[38]

An interesting extension of this spectroscopy would be scanning the visible frequency to create a resonance IR excitation spectrum analogous to a resonance Raman excitation spectrum. Such an experiment would yield information assisting in assignment of both electronic and vibrational states. Resonance Raman spectroscopy has been used extensively to follow processes like electron-transfer dynamics and photo-induced conformational changes,[1] and TRSF spectroscopy will have analogous but complementary capabilities. It has been shown that electron-transfer processes are assisted by asymmetric modes, while symmetric modes contribute to Marcus theory reorganization energy.[39] Therefore, electronic enhancement of IR-active modes provides a useful probe of electron-transfer processes because the relevant vibrations may be absent or more poorly enhanced in resonance Raman. Application of this technique to low-symmetry species could still provide greater insight. For example, comparison of the excitation profiles of a combination band and a diagonal feature could lend insight into multimode effects[5] that are difficult to

dx.doi.org/10.1021/jp5018554 | J. Phys. Chem. A 2014, 118, 3112–3119

quantify in the combination bands of one-dimensional Raman spectra.

One could also take advantage of the ability to resolve mechanical coupling strength by looking at cross-peak anharmonicity[21] to learn about structural differences between sites of interest. The multidimensional aspect of the TRSF experiment would also distinguish between vibrations found at different sites in the sample even if electronic absorption at those sites occurs at the same frequency because only functional groups at the same site would share a cross-peak. Another new possibility is the potential to use polarized excitation beams to learn about the relative orientation of transition dipoles, as is done in other multidimensional vibrational experiments.[40,41] TRSF capabilities should therefore bridge and complement those provided by methods like 2D-IR and resonance Raman spectroscopy.

■ ASSOCIATED CONTENT

Ⓢ Supporting Information

The Supporting Information contains the ATR FTIR spectrum, infrared molar absorptivities, resonance Raman spectra in the overtone region, an overlay of the TRSF diagonal with the ATR spectrum and square of the visible absorption spectrum, and a discussion and modeling of the effects of refractive index dispersion and sample absorption on the TRSF spectra. This material is available free of charge via the Internet at http://pubs.acs.org.

■ AUTHOR INFORMATION

Corresponding Author

*E-mail: wright@chem.wisc.edu. Phone: 608-262-0351.

Notes

The authors declare no competing financial interest.

■ ACKNOWLEDGMENTS

We would like to thank Prof. Thomas Brunold for valuable insight and Beth Blaesi for assistance with ORCA. This material is based upon work supported by the National Science Foundation Division of Chemistry under Grant No. 1057896 (Chemical Measurement and Imaging, with cofunding from the Chemical Structures, Dynamics, and Mechanisms program) and by the Department of Defense (DoD) through the National Defense Science & Engineering Graduate Fellowship (NDSEG) Program.

■ REFERENCES

(1) Schoonover, J. R.; Strouse, G. F. Time-Resolved Vibrational Spectroscopy of Electronically Excited Inorganic Complexes in Solution. *Chem. Rev.* **1998**, *98*, 1335−1355.

(2) Czernuszewicz, R. S.; Spiro, T. G. *Inorganic Electronic Structure and Spectroscopy*; John Wiley & Sons: New York, 1999; pp 353−441.

(3) Van Heuvelen, K. M.; Kieber-Emmons, M. T.; Riordan, C. G.; Brunold, T. C. Spectroscopic and Computational Studies of a *trans*-μ-1,2-Disulfido-Bridged Dinickel Species, $\{(tmc)Ni\}_2(S_2)(OTf)_2$: Comparison of End-on Disulfido and Peroxo Bonding in $(Ni^{II})_2$ and $(Cu^{II})_2$ Species. *Inorg. Chem.* **2010**, *49*, 3104−3112.

(4) Han, J.; Loehr, T. M.; Lu, Y.; Valentine, J. S.; Averill, B. A.; Sandersloehr, J. Resonance Raman Excitation Profiles Indicate Multiple CuS−Cu Charge-Transfer Transitions in Type-I Copper Proteins. *J. Am. Chem. Soc.* **1993**, *115*, 4256−4263.

(5) Spiro, T.; Czernuszewicz, R., Resonance Raman Spectroscopy. In *Physical Methods in Bioinorganic Chemistry*; Que, L., Ed.; University Science Books: South Orange, NJ, 2000; pp 85−95.

(6) Van Heuvelen, K. M.; Cho, J.; Dingee, T.; Riordan, C. G.; Brunold, T. C. Spectroscopic and Computational Studies of a Series of High-Spin Ni(II) Thiolate Complexes. *Inorg. Chem.* **2010**, *49*, 6535−6544.

(7) Stich, T. A.; Buan, N. R.; Brunold, T. C. Spectroscopic and Computational Studies of Co^{2+} Corrinoids: Spectral and Electronic Properties of the Biologically Relevant Base-on and Base-off Forms of Co^{2+} Cobalamin. *J. Am. Chem. Soc.* **2004**, *126*, 9735−9749.

(8) Sorokin, A. B. Phthalocyanine Metal Complexes in Catalysis. *Chem. Rev.* **2013**, *113*, 8152−8191.

(9) Schumann, S.; Hatton, R. A.; Jones, T. S. Organic Photovoltaic: Devices Based on Water-Soluble Copper Phthalocyanine. *J. Phys. Chem. C* **2011**, *115*, 4916−4921.

(10) Basova, T. V.; Kiselev, V. G.; Schuster, B.-E.; Peisert, H.; Chasse, T. Experimental and Theoretical Investigation of Vibrational Spectra of Copper Phthalocyanine: Polarized Single-Crystal Raman Spectra, Isotope Effect and DFT Calculations. *J. Raman Spectrosc.* **2009**, *40*, 2080−2087.

(11) Mukamel, S. *Principles of Nonlinear Optical Spectroscopy*; Oxford University Press: New York, 1999.

(12) Wright, J. C. Multiresonant Coherent Multidimensional Spectroscopy. *Annu. Rev. Phys. Chem.* **2011**, *62*, 209−230.

(13) Donaldson, P. M.; Fournier, F.; Gardner, E. M.; Barter, L. M. C.; Palmer, D. J.; Klug, D. R. Multidimensional Infrared Spectroscopy — The Optical Analogue of 2D NMR. In *International Conference on Coherent Multidimensional Spectroscopy*; Rigi Kulm, Switzerland, 2006.

(14) Pakoulev, A. V.; Rickard, M. A.; Meyer, K. A.; Kornau, K.; Mathew, N. A.; Thompson, D. E.; Wright, J. C. Mixed Frequency/Time Domain Optical Analogues of Heteronuclear Multidimensional NMR. *J.Phys. Chem. A* **2006**, *110*, 3352−3355.

(15) Zanni, M. T.; Hochstrasser, R. M. Two-Dimensional Infrared Spectroscopy: A Promising New Method for the Time Resolution of Structures. *Curr. Opin. Struct. Biol.* **2001**, *11*, 516−522.

(16) Shim, S. H.; Strasfeld, D. B.; Ling, Y. L.; Zanni, M. T. Automated 2D IR Spectroscopy Using a Mid-IR Pulse Shaper and Application of This Technology to the Human Islet Amyloid Polypeptide. *Proc. Natl. Acad. Sci. U.S.A.* **2007**, *104*, 14197−14202.

(17) Rubtsov, I. V.; Kumar, K.; Hochstrasser, R. M. Dual-Frequency 2D IR Photon Echo of a Hydrogen Bond. *Chem. Phys. Lett.* **2005**, *402*, 439−443.

(18) Zhao, W.; Wright, J. C. Doubly Vibrationally Enhanced Four Wave Mixing: The Optical Analog to 2D NMR. *Phys. Rev. Lett.* **2000**, *84*, 1411−1414.

(19) Besemann, D. M.; Meyer, K. A.; Wright, J. C. Spectroscopic Characteristics of Triply Vibrationally Enhanced Four-Wave Mixing Spectroscopy. *J. Phys. Chem. B* **2004**, *108*, 10493−10504.

(20) Boyle, E. S.; Pakoulev, A. V.; Wright, J. C. Fully Coherent Triple Sum Frequency Spectroscopy of a Benzene Fermi Resonance. *J.Phys. Chem. A* **2013**, *117*, 5578−5588.

(21) Boyle, E. S.; Neff-Mallon, N. A.; Wright, J. C. Triply Resonant Sum Frequency Spectroscopy: Combining Advantages of Resonance Raman and 2D-IR. *J. Phys. Chem. A* **2013**, *117*, 12401−8.

(22) Carlson, R. J.; Wright, J. C. Absorption and Coherent Interference Effects in Multiply Resonant Four-Wave Mixing Spectroscopy. *Appl. Spectrosc.* **1989**, *43*, 1195.

(23) Neese, F. *Orca 2.9.1, An Ab Initio, DFT, and Semiempirical Electronic Structure Package*.

(24) Becke, A. D. A New Mixing of Hartree−Fock and Local Density-Functional Theories. *J. Chem. Phys.* **1993**, *98*, 1372−1377.

(25) Becke, A. D. Density-Functional Thermochemistry 3. The Role of Exact Exchange. *J. Chem. Phys.* **1993**, *98*, 5648−5652.

(26) Lee, C. T.; Yang, W. T.; Parr, R. G. Development of the Colle−Salvetti Correlation Energy Formula Into a Functional of the Electron Density. *Phys. Rev. B* **1988**, *37*, 785−789.

(27) Schafer, A.; Horn, H.; Ahlrichs, R. Fully Optimized Contracted Gaussian Basis Sets for Atoms Li to Kr. *J. Chem. Phys.* **1992**, *97*, 2571−2577.

(28) Weigend, F.; Haser, M. RI-MP2: First Derivatives and Global Consistency. *Theor. Chem. Acc.* **1997**, *97*, 331−340.

(29) Schafer, A.; Huber, C.; Ahlrichs, R. Fully Optimized Contracted Gaussian Basis Sets of Triple Zeta Valence Quality for Atoms Li to Kr. *J. Chem. Phys.* **1994**, *100*, 5829−5835.
(30) Afanasiev, P.; Kudrik, E. V.; Albrieux, F.; Briois, V.; Koifman, O. I.; Sorokin, A. B. Generation and Characterization of High-Valent Iron Oxo Phthalocyanines. *Chem. Commun.* **2012**, *48*, 6088−6090.
(31) Camp, P. J.; Jones, A. C.; Neely, R. K.; Speirs, N. M. Aggregation of Copper(II) Tetrasulfonated Phthalocyanine in Aqueous Salt Solutions. *J.Phys. Chem. A* **2002**, *106*, 10725−10732.
(32) Abramczyk, H.; Szymczyk, I. Aggregation of Phthalocyanine Derivatives in Liquid Solutions and Human Blood. *J. Mol. Liq.* **2004**, *110*, 51−56.
(33) Liao, M. S.; Scheiner, S. Electronic Structure and Bonding in Metal Phthalocyanines, Metal=Fe, Co, Ni, Cu, Zn, Mg. *J. Chem. Phys.* **2001**, *114*, 9780−9791.
(34) Gouterman, M. *The Porphyrins*; Dolphin, D., Ed.; Academic Press: New York, 1979; Vol. *III*, pp 1−156.
(35) Szymczyk, I.; Abramczyk, H. Peripheral Substituent and Solvent Effects on the Aggregation and Photochemical Properties of Copper(II) Phthalocyanine and Copper(II) Phthalocyanine-3,4 ′,4 ″,4 ‴-Tetrasulfonic Anion. *Pure Appl. Chem.* **2004**, *76*, 183−187.
(36) Brozek-Pluska, B.; Szymczyk, I.; Abramczyk, H. Raman Spectroscopy of Phthalocyanines and Their Sulfonated Derivatives. *J. Mol. Struct.* **2005**, *744*, 481−485.
(37) Paulat, F.; Praneeth, V. K. K.; Nather, C.; Lehnert, N. Quantum Chemistry-Based Analysis of the Vibrational Spectra of Five-Coordinate Metalloporphyrins M(TPP)Cl. *Inorg. Chem.* **2006**, *45*, 2835−2856.
(38) Tang, J.; Albrecht, A. C. Developments in the Theories of Vibrational Raman Intensities. In *Raman Spectroscopy: Theory and Practice*; Szymanski, H. A., Ed.; Plenum Press: New York, 1970; Vol. *2*, pp 33−68.
(39) Bailey, S. E.; Zink, J. I.; Nelsen, S. F. Contributions of Symmetric and Asymmetric Normal Coordinates to the Intervalence Electronic Absorption and Resonance Raman Spectra of a Strongly Soupled *p*-Phenylenediamine Radical Cation. *J. Am. Chem. Soc.* **2003**, *125*, 5939−5947.
(40) Chen, H.; Zhang, Y.; Li, J.; Liu, H.; Jiang, D.-E.; Zheng, J. Vibrational Cross-Angles in Condensed Molecules: A Structural Tool. *J. Phys. Chem. A* **2013**, *117*, 8407−8415.
(41) Hochstrasser, R. M. Two-Dimensional IR-Spectroscopy: Polarization Anisotropy Effects. *Chem. Phys.* **2001**, *266*, 273−284.